OPEN ACCESS
IOP Publishing
Measurement Science and Technology
Meas. Sci. Technol. **30** (2019) 104001 (12pp)
https://doi.org/10.1088/1361-6501/ab24a1

A customized multispectral needle probe combined with a virtual photometric setup for *in vivo* detection of Lewis lung carcinoma in an animal model

Frank Braun[1], Robert Schalk[1], Marcel Nachtmann[1], Andreas Hien[1], Rudolf Frank[1], Thomas Beuermann[2], Frank-Jürgen Methner[3], Bettina Kränzlin[4], Matthias Rädle[1,5] and Norbert Gretz[4,5]

[1] Center for Mass Spectrometry and Optical Spectroscopy, Mannheim University of Applied Sciences, Paul-Wittsack-Str. 10, 68163 Mannheim, Germany
[2] Institute for Process Control, Mannheim University of Applied Sciences, Paul-Wittsack-Str. 10, 68163 Mannheim, Germany
[3] Institute of Biotechnology, Technical University of Berlin, Chair of Brewing Science, Berlin, Germany
[4] Medical Research Center, University of Heidelberg, Theodor-Kutzer-Ufer 1-3, 68167 Mannheim, Germany

E-mail: m.raedle@hs-mannheim.de

Received 2 January 2019, revised 13 May 2019
Accepted for publication 24 May 2019
Published 8 August 2019

Abstract

Optical systems applied for tissue analysis are primarily based on single spectroscopic techniques. This paper however presents a multispectral backscattering sensor designed for *in vivo* application by a specially formed probe tip which allows side by side monitoring of ultraviolet, visible, near-infrared and fluorescence spectra. The practical applicability of the measurement system was demonstrated *in vitro* (muscle and adipose tissue) and *in vivo* in an animal model (mouse). By comparing associated measuring changes in biochemical, physical-morphological and colorimetric values this procedure allows a differentiation between healthy, marginal and malignant tissue.

Keywords: multispectral needle probe, UV/VIS/NIR/fluorescence (FL) tissue spectroscopy, *in vivo* cancer/carcinoma/diagnostics, animal model for Lewis lung cancer, Nitinol fiber-optic probe for oncology, photometric setup

Supplementary material for this article is available online

(Some figures may appear in colour only in the online journal)

[5] Norbert Gretz and Matthias Rädle contributed equally to this work.

1. Introduction

Cancer ranks number two among the causes of death annually; more than 14 million new diagnosed cases occurred in 2012 [1]. Estimations forecast that over 22.2 million cases will occur in 2030 [2]. The challenge is to detect malignant neoplasia at an early stage to increase the probability of cure. Therefore, many efforts have been undertaken to improve the detection of tissue changes. Classical diagnostic methods range from palpation, imaging methods such as MRI, scintigraphy or computed tomography, to immunological methods. To date, different biopsy techniques with subsequent evaluation by a pathologist based on microscopy images in a laboratory are the gold standard for diagnosis of tissue alterations [3, 4]. The biopsy procedure is one of the most frequently performed clinical interventions [5]. Each histopathological examination is usually carried out by hand—not automatically, and generally very cost intensive. In such cases, optical spectroscopy, especially for prevention and early diagnosis, offers benefits as a minimally invasive preselection and supporting tool implemented during the biopsy procedure.

Optical spectroscopic techniques for the detection of cancer have become of increasing interest since the 1990s. The state-of-the-art of the respective developments is summarized. The sample preparations range from cooled, shock-frozen [6, 7], formalin-fixed paraffin-embedded (FFPE) sections to unfixed frozen or fresh tissue [8]. Pancreatic and colorectal cancer have been detected in fresh biopsies without post-treatment using near infrared (NIR) spectroscopy [9, 10].

The analyses are mainly based on the determination of the tissue composition, such as water [11], fat [12, 13], collagen [14, 15] or hemoglobin (Hb) [16]. In addition, oxygen saturation or the oxygen requirement of tissue can be used [17]. The content of the red blood pigment Hb is an important marker in cancer diagnosis and is detectable *in vivo* via fiber optical spectroscopy. Solid tumors depend on a growing capillary network (tumor-induced angiogenesis), which supplies the tumor with oxygen and nutrients. For growth beyond a volume of 1 to 2 mm^3, the formation of new blood vessels is necessary. Without this opportunity for nourishment, non-angiogenic neoplasias are restricted to a symptomless and not clinically relevant size [18]. The results of Chen *et al* [19] indicate that within each patient, the average Hb level in a brain tumor is relatively higher than the average Hb measured in the normal cortex. The overall average of six patients was $0.37 \pm 0.18\,g\,dl^{-1}$ in the normal cortex and $0.99 \pm 0.57\,g\,dl^{-1}$ in tumor tissue [19]. Because Hb is a strong VIS and NIR radiation absorber, spectral data are used as a reference for blood flow [20]. To evaluate the concentration of connective tissue, it is best to choose a spectral range with a low absorbance in the 'optical window of tissue' [21, 22] using elastic light scattering techniques [22].

In addition to absorption methods, fluorescence (FL) emission diagnostics are commonly used to recognize skin [23], bladder [24], lung [25], and cervical [26] cancer. In this spectroscopic technique, nicotinamide adenine dinucleotide hydrate (NADH) is a significant marker [27–30]. NADH FL serves as an indicator of cell metabolism and redox state as well as of oxygen deficiency and disorders in the respiratory chain [31, 32]. An increase in the NADH concentration and thus its FL emission signal indicates a decline in tissue activity and a concomitant low NADH consumption [33]. In contrast, a decreased concentration in tissue shows an increase in metabolic cell activity [34]. The change of NADH concentrations are generally used for tumor localization, because tumorous tissue has a reduced FL compared with normal tissue [26]. In addition, FL-spectroscopy can be combined with diffuse reflection, as described in a publication relating to the detection of cervical cancer precursors *in vivo* [35].

Based on the current state of the art and the various methods as described we saw great potential in combining several spectral methods (UV/VIS, NIR, FL) in one multispectral *in vivo* probing system for several purposes: to shorten the time of the diagnosis, to reduce the numbers of surgical interventions, thus making it—if put to practice—less stressful for patients, and hopefully more economic. As a valuable example and a model for our evaluations we have chosen mice with Lewis lung cancer and compared our detection methods with clinical results.

2. Materials and methods

2.1. Animal model and procedure

As a mice model, the well-known and reproducible model Lewis lung carcinoma is used. Female SPF NMRI mice (approximately 12 weeks old) were purchased from Janvier-Labs (Le Genest St. Isle, France) and provided with free access to standard food and water. *In vivo* experiments were performed according to EC directive 2010/63 EU. Six mice were injected subcutaneously in the flank region with 5×10^5 LLC P4 cells/mouse (Lewis lung carcinoma cells in 100 µl of phosphate-buffered saline solution). After approximately 2 weeks, the carcinoma *in situ* had grown to a size of approximately 1 cm^3, which allowed us to examine the animals under anesthesia (medetomidine 0.5 mg kg^{-1} BW (Eurovet/Albrecht GmbH, Aulendorf, Germany), midazolam 5 mg kg^{-1} BW (Ratiopharm GmbH, Ulm, Germany), fentanyl, 0.05 mg kg^{-1} BW (Janssen Cilag, Neuss, Germany)). After shaving and disinfection of the skin, a small skin cut of approximately 1–2 mm in the vicinity of the tumor allowed minimal invasive entry of the multispectral needle. Throughout the procedure, the temperature of the animals was kept constant using a warming plate. In addition, an *in vitro* pilot test was performed stitching in adipose and muscle tissue samples. The observed measurement effects are explained in detail in section 3.2, performing an *in vitro* pilot test of tissue samples.

2.2. Measurement setup for multispectral analysis

The multispectral *in vivo* measurement setup is illustrated schematically in figure 1.

The fluorescence of the sample was excited with a light emitting diode (purple) (365 nm LED, NCSU 033B, Nichia, Tokushima, Japan) and the corresponding fluorescence emission spectrum was detected using a MCS CCD/UV-NIR

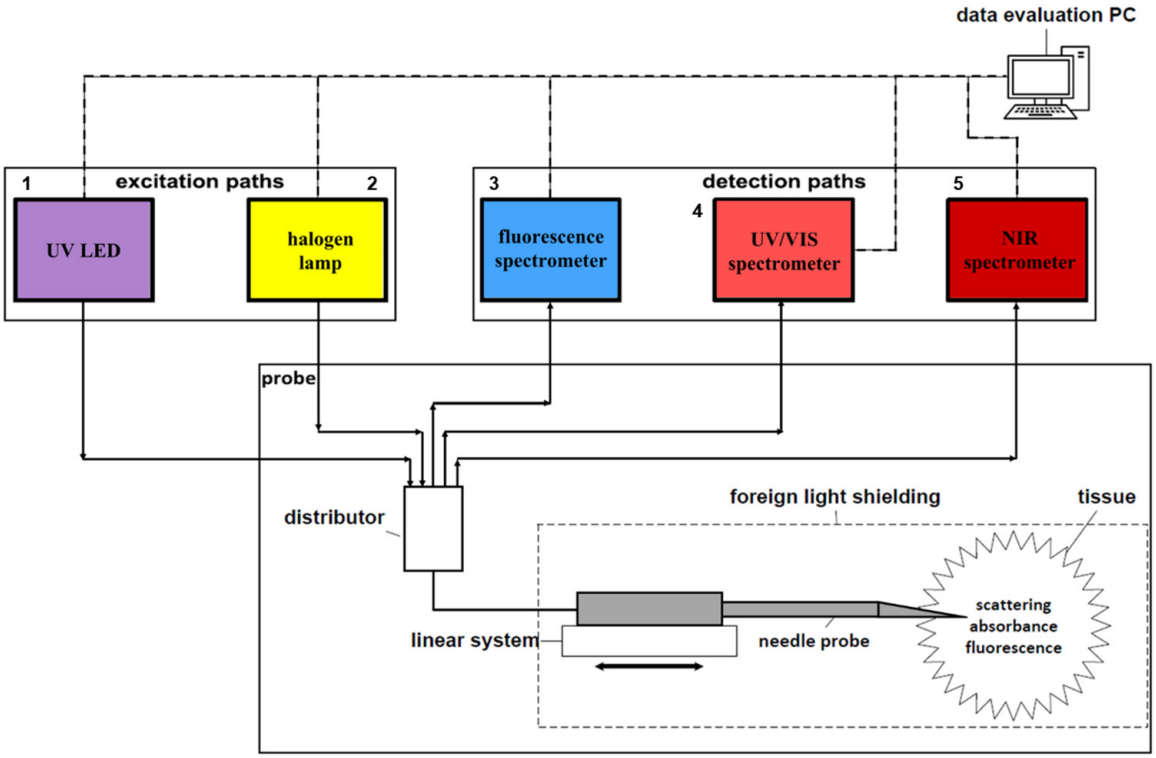

Figure 1. Remission measurement setup for multispectral *in vivo* tissue analysis. The setup consisted of two light sources, three spectrometers and a multispectral needle probe to obtain UV/VIS, NIR-remission and fluorescence emission spectra. The coloring and numbering represents the coding for the connection, see also figure 2.

spectrometer from Carl Zeiss AG, Jena in Germany. The LED is an UV-light emitting diode with an emission maximum at 365 nm and a spectrum half width of 9 nm. The optical power output measured at the probe head is approximately 160 μW. The LED was externally triggered and emits light only in the integration time of the fluorescence measurement sequence. Subsequently, this spectrometer is named as fluorescence spectrometer (blue). In order to induce the sample's absorbance, a broadband halogen lamp (yellow) (CLH 600, Carl Zeiss AG, Jena, Germany) is utilized. The color temperature of a Planckian radiation illuminant *A* is 2854 K, as specified by the International Commission on Illumination (CIE). The tungsten–halogen luminaire has a similar color temperature of 2900 K, as specified by the manufacturer. To minimize the photon flux on the sample the luminaire is operated in a special mode: The shutter is only opened for integration time of the momentary measuring sequence. Furthermore, the light source is very weak and is strongly attenuated by an SMA coupling with only 200 microns core-diameter.

The absorbance spectra were calculated based on remission spectra recorded with the aid of two spectrometers. While one spectrometer detected the remitted light in the UV/VIS-range (light red) (MCS 621 VIS II, Carl Zeiss AG, Jena, Germany), the other spectrometer was used to measure the remission spectrum in the NIR range (red) (MCS611 NIR 2.2, Carl Zeiss AG, Jena, Germany). The spectra were recorded with different integration times (100 ms for UV/VIS, 200 ms for NIR and 250 ms for FL spectroscopy) using the software Aspect Plus® (Version 2.3, Carl Zeiss AG, Jena, Germany). The reference material used is a Spectralon® Diffuse Reflectance Standard (SphereOptics GmbH, Herrsching, Germany), with a Lambertian reflectance value of 99% and a constant reflection of ±4% over the wavelength range of 250 nm–2500 nm. The measurement sequence was started with FL followed by UV/VIS and NIR measurements with continuous dark current correction and then by analysis with Unscrambler® X (CAMO Software AS, Norway) as the multivariate analytical software. To exclude autoFL in the setup and ambient light, the measuring arrangement was shielded by two layers (black fabric as the outer layer and carbon black polymer foil as the inner layer). For a higher signal-to-noise ratio, mean values were calculated from three measurement data sets.

As a measurement probe, a multispectral needle is used to obtain the different spectra. This probe was connected to the light sources and the spectrometers via optical fibers. A detailed description of the probe is given in the following section. For precise movement along the axis, the probe was attached to a linear system (Spindler & Hoyer, Göttingen, Germany).

The entire setup, including the multispectral needle, was evaluated by UV/VIS, NIR and FL measurements in a liquid tissue phantom [22, 36]. Additionally, its MRI capability was confirmed by measurements tracking the needle position in a biological phantom [22].

2.3. Design of the needle probe for multispectral in vivo diagnostics

The probe consisted of seven quartz fibers (numerical aperture (NA) 0.22, core/outer-diameter: 200/250 μm, Edmund

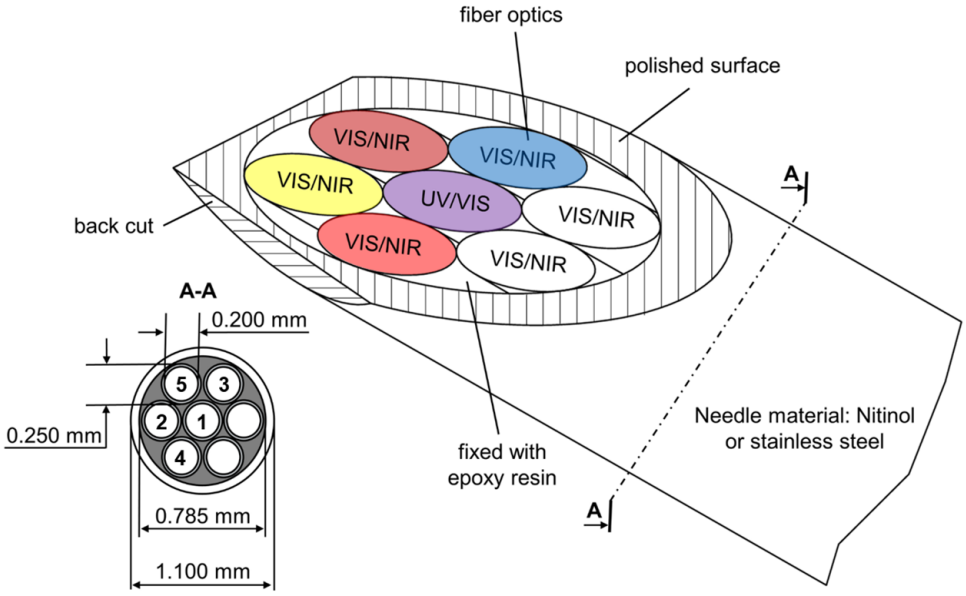

Figure 2. Optimized multispectral needle for efficient tissue penetration: cut at a 30° angle, including a back-cut bevel. The circularly arranged fibers are inside the 19 G cannula, e.g. one UV/VIS fiber for FL excitation and six VIS/NIR fibers; see also figure 1. The dimensions of the needle and the optical fibers are illustrated at the bottom left. The coloring and numbering represents the coding for the connection; see also figure 1.

Optics Ltd, York, UK) that were stuck together in the probe head. Adapted to the application, an epoxy resin (EPO-TEK® 353ND, Epoxy Technology Inc., Billerica, USA certified to USP Class VI and ISO 10993 biocompatibility standards for medical implants) was used to fill the gaps and fix the fibers, shown in figure 2. This adhesive is also compatible with the CIDEX® OPA sterilization standard.

The optical fibers were bundled in one ultrasound- and MRI-compatible 1.1 mm 19 G needle probe (inner diameter 0.785 mm, stainless steel cannula, Sterican, B. Braun AG, Melsungen, Germany) or Nitinol capillary [37–39] (Endosmart® Gesellschaft für Medizintechnik mbH, Stutensee, Germany) with a special beveled head designed similarly to a hypodermic needle for efficient penetration into the tissue. The inner fiber was optimized for the UV/VIS region (high OH content) and was used for FL excitation, and the surrounding six fibers were ideally suited for the VIS/NIR region (low OH content). The combination of different optical properties in one probe head enabled the application of various spectroscopic techniques side by side *in vivo* nearly simultaneously without changing the setup. Using a distributor, the seven optical fibers were separated into shielded channels, which generally enable an individual and simultaneous selection of light sources and spectrometers or other detectors via the SMA connection [40]. The penetration depth of the needle in a liquid tissue phantom with similar scattering coefficients, such as human pale forearm skin (Fitzpatrick scale Type II), was approximately 0.8 mm [22]. The probe setup was well suited not only for the presented investigation but also shows benefits for future applications as described: easy tissue penetration by a plane-ground head cut at a 30° angle and a back-cut bevel (figure 2), manufactured from biocompatible materials, which allow multiple use by autoclaving and re-sharpening. Multi-wavelengths excitations or the implementation of further detection channels are possible for real-time measurement during the biopsy procedure. More details and a local *in vivo* pulse measurement are shown in the supporting information (stacks.iop.org/MST/30/104001/mmedia).

2.4. Tracking of the needle position with ultrasound and specific marking with a filament

In our investigation, the needle was tracked using a standard ultrasound system (Philips Sonos 5500, Philips Medical System, Hamburg, Germany) with the following attributes: depth setting 2 cm, frequency 76 Hz; and a Philips 15-6L linear probe. During the application, the gel layer thickness between the probe and skin was in the centimeter range to overcome the minimum clearance for measuring tissue directly under the surface. To identify the position of the puncture channel, the needle was clearly marked with a polymer filament (PROLENE, Johnson & Johnson Medical GmbH, Norderstedt, Germany) attached with UV adhesive (Bondic®, VIKO UG, Munich, Germany) on the side of the probe head. The filament remained in the puncture channel for histopathology after the probe was removed.

2.5. Preprocessing and data reduction of the multispectral information by a virtual photometric structure

The recorded multispectral data (UV/VIS, NIR and FL) are preprocessed by an application-driven method for data reduction. This method follows the step of the data acquisition. The enormous amount of spectroscopic data generated (40 000 bytes per measuring point) is reduced by this specialized virtual photometer structure to five specific measurement channels (figure 3).

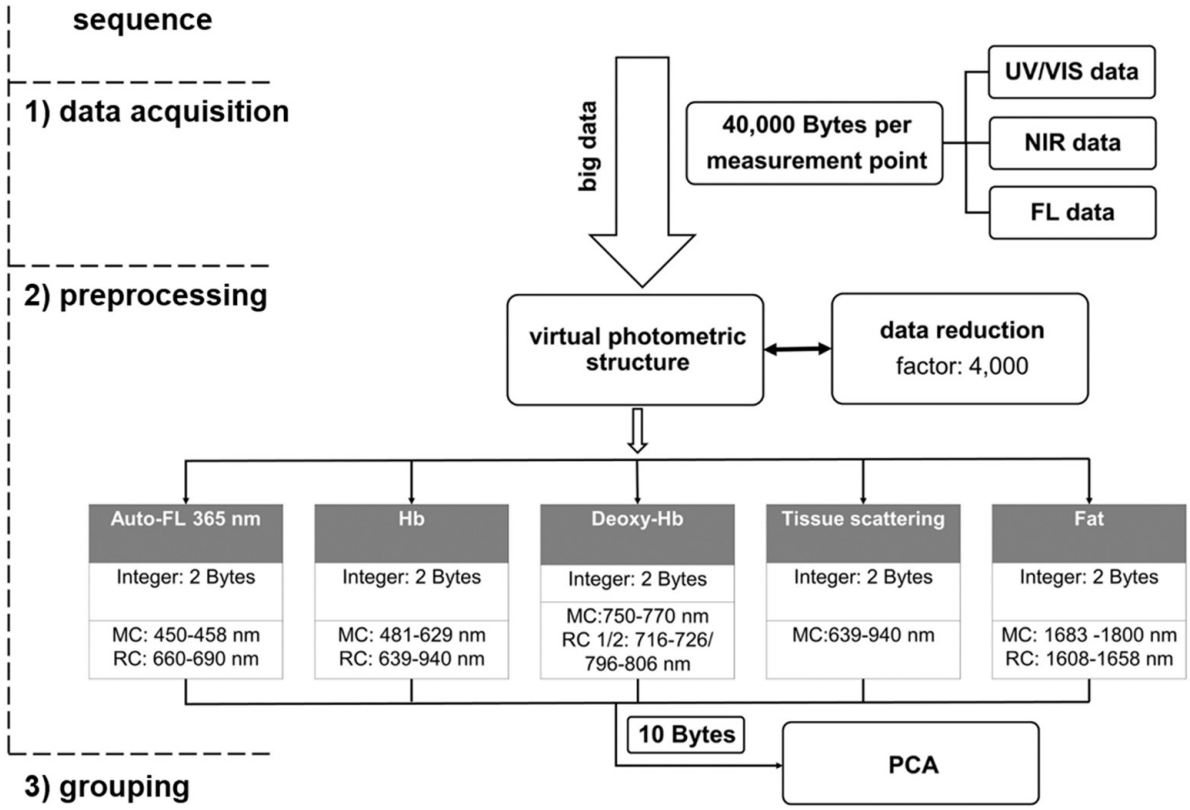

Figure 3. Preprocessing of the multispectral data by a virtual photometric structure and grouping by PCA.

The data type is an integer with two bytes per measurement point and channel. The calculation was performed with basic mathematical operations to use the hardware as efficiently as possible. Thus, the spectral amount of data was reduced by a factor of 4000—shown in figure 3. At a sampling rate of 50 Hz, which corresponds to 3000 measuring points min^{-1}, the amount of data before reduction is 120 megabytes min^{-1}. After preprocessing, it was reduced to 0.03 megabytes min^{-1} of system operating time. The flow chart for the described application is illustrated in figure 3, including all summed-up bandpasses and their wavelength-ranges for measurement (MC) and reference channels (RC).

The channels were systematically selected from spectral regions of high variance and the respective measurement effect were assigned by literature. All channels, see figure 3, are determined by integration over the wavelength areas and if necessary factorized for weighting. The measurements channels subtracted by the reference channel result in each channel.

The auto-FL-365 nm channel is based on a measuring and a reference channel. The measuring channel detects the maximum auto fluorescence emission. To compensate the background a reference channel at longer wavelength region is chosen.

The measuring channel of the red blood pigment Hb lies in the green absorption region. As a reference for offset compensation serves the optical window of tissue, which is dominated by physical scattering and minimal absorption effects. As a result, the matrix effect caused by scattering can be compensated.

The deoxy form of Hb has a low absorption band within the optical window of tissue. This absorption has distinct advantage to other associated bands—no overlapping. The result is a highly selective measurement. Since the measuring effect is small, a very good compensation of the background is important. For this reason, a reference channel was set both short- and long-wave, and the mean was subtracted from the measuring channel. In order to capture the tissue scattering as purely as possible, the optical window between Hb and water absorption is selected. This region of least tissue absorption is largely dominated by scattering. Here, one measuring channel was set, a reference channel would falsify or even eliminate the target variable scattering. To detect fat, the measuring channel was placed on the characteristic band of fatty tissue and a short-wave reference was chosen to compensate the background. As a result, pseudo-absorption effects caused by scattering can be compensated.

2.6. Grouping of the reduced data via multichannel PCA

PCA is a statistical method used to reduce multidimensional data to principal components (PCs). The resulting lower dimensional coordinate system describes the recorded spectral data from the different techniques applied, UV/VIS, NIR and FL spectroscopy, in the form of five specific measurement sensors/channels. The impact of each individual channel variable on a PC is expressed in the loading spectra. The channels themselves are described by their score values in the new PC coordinate system.

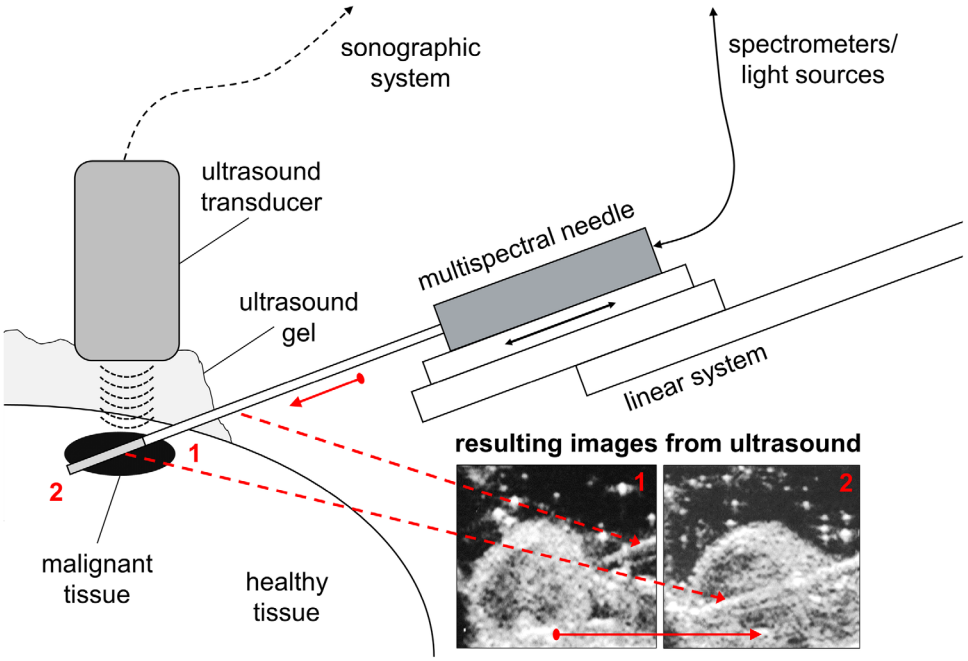

Figure 4. Ultrasonic tracking of the cannula position. The sonograms, labeled 1 and 2, show the needle probe and the typical metal echogenic artifacts at different positions: position 1 before penetrating the malignant tissue and position 2 after the stitch procedure at the end position.

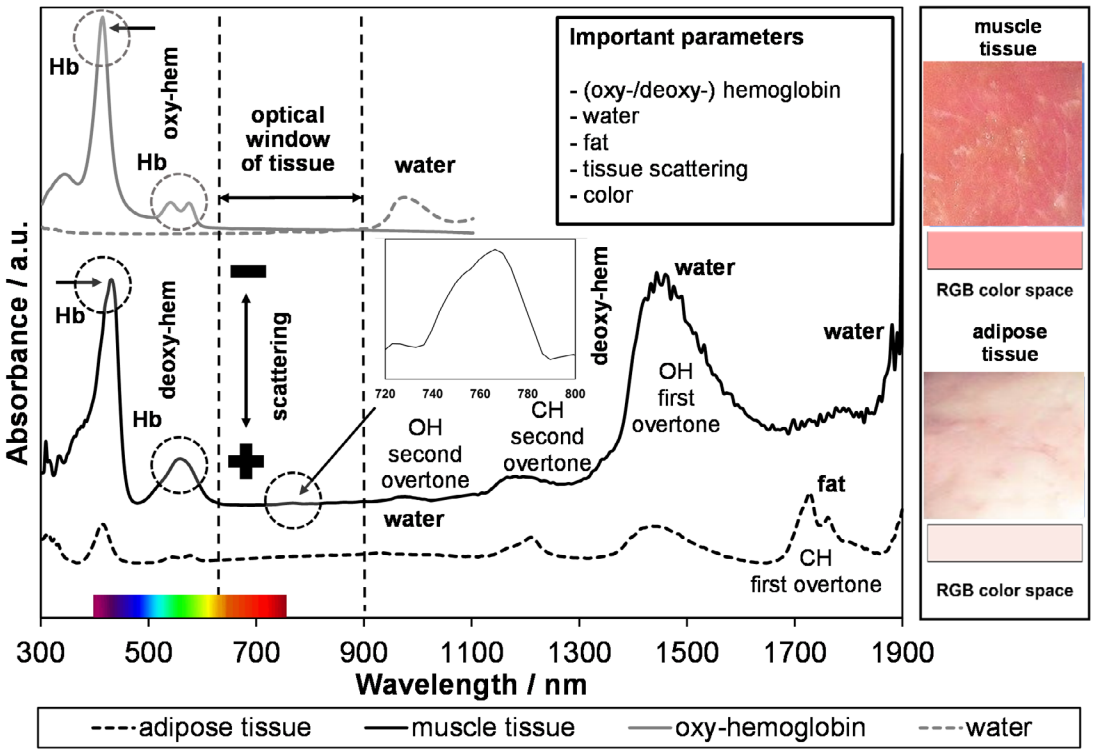

Figure 5. Simultaneously generated VIS/NIR absorbance spectra of muscle and adipose tissue using the multispectral needle probe. The optical window between oxy-hemoglobin and water is illustrated on the top left. In addition, the upper photo shows a direct measurement, and the lower photo shows the color calculation.

The principle is shown in matrix notation [41]:

$$X = TP^T + E$$

$X = data\ matrix$ (*lines are the samples*; columns are the spectral values)

$T = scorematrix$ (*describing the samples* : weighting)

P^T = transposed *loadingmatrix* (summarizes channel data : variables)

E = residual matrix (unexplained share : *noise*, *error*).

3. Results

3.1. Tracking of the multispectral needle probe and marking of the stitch pathway

The live ultrasonic pictures of the probe during the tissue penetration (from right to left) are illustrated in figure 4.

The probe position was detectable by echogenic signals and thus was known at any given time. This is a live *in vivo* tracking of the needle in the mouse model study. The two solid red arrows next to the probe and the pictures indicate the stich position before and after.

Samples were collected and evaluated by a pathologist and the spectra were correlated with the respective tissue. The combination of all three techniques (ultrasound pictures, measurement of the penetration depth using the scale on the linear system, and marking of the stitch pathway by a textile fiber for the subsequent gold standard pathological medical report) led to the presented correlations. Thus, the verification was guaranteed whether the measurement was carried out inside or outside the tumor or in an intermediate tissue region.

3.2. Performing an in vitro pilot test of tissue samples

Exemplary adipose and muscle tissue probes were stitched, and spectral information was generated from dead tissue (figure 5). For the purpose of our investigations untreated pork tissue was used.

Through illumination with a broadband halogen light source, the scattering and absorption characteristics over a wide range from 200–1900 nm were detectable. The dominant absorption peaks near 430 nm and 560 nm are characteristic for blood pigment (Hb). In comparison with adipose tissue, muscle tissue has a higher supply of blood and thus exhibits a high spectral absorbance in the green spectral range and is visually recognizable by its red color. The optical window and the oxygen-loaded Hb spectral data are shown at the top left. The aqueous highly diluted blood Hb and pure water spectrum is generated in a transmission setup using a 10 mm cuvette inserted in a cuvette-holder (Hellma GmbH & Co. KG, Müllheim, Germany). The backscattering signal inside the adipose tissue was much stronger than that from muscle tissue, as demonstrated by the low absorption in the VIS spectrum. The three specific and broad water peaks, which appear at approximately 980, 1444 and 1944 nm [11], can be found in both tissues; however, they are more dominant in muscle tissue [42]. The absorption bands of the fatty acids were distinctive in the NIR region at approximately 920, 1040, 1210, 1730, and 1760 nm [43]. In addition to the spectral data for muscle and adipose tissue, a supplementary photo, including calculated RGB color from the spectral data, is provided on the right side of figure 5. The photos were taken with a digital camera and are used for visualization. Color values are calculated by using the embedded color-function of ASPECT PLUS (Carl Zeiss Spectroscopy GmbH, Jena, Germany). These explained optical (morphological and chemical) properties are of utmost importance for the subsequent point described in the next section.

3.3. Proof of concept: multispectral label-free in vivo grouping of healthy and malignant tissue

For grouping of healthy and malignant tissue, *in vivo* measurements were conducted in an animal model using the multispectral needle probe. Figure 6 shows the spectral data for the three spectroscopic techniques, UV/VIS, NIR and FL. These are exemplary spectra of a single mouse. The spectral information are the first acquired data in the sequence chain.

Through the identification of differences in the optical properties of healthy, marginal and malignant tissue the channels in figure 3 are selected. The multispectral information content is described above. The following biochemical and morphological properties were determined using the multispectral measuring system. The FL spectra include excitation by the 365 nm LED light source as additional information. The LED shows strong absorption in malignant tissue, which is mainly caused by the enhanced Hb absorption. The FL emission at approximately 460 nm is much lower for malignant tissue than for marginal and surrounding healthy tissue. Furthermore, the UV/VIS, NIR spectral data exhibit differences. A higher absorbance generally indicates less backscattering signal. In contrast, more scattering, which depends on the morphology of the involved components (size, structure, inner surface of the tissue) results in lower absorption (almost untouched by the chemical absorption in the optical window of the tissue between 650–900 nm). The interaction of scattering effects and the overlying spectrum of blood (mainly Hb) reveals that the total Hb content in malignant tissue is increased in contrast to the surrounding tissue. Additional information is provided by the reduced oxygen saturation in this tissue. The effects are summarized in the following section and are demonstrated visually in figure 6: the increased peak at 560 nm indicates higher Hb loading. The absorption maximum at approximately 430 nm is shifted to the right, which indicates less oxygen saturation due to a decreased oxy-/deoxy-Hb ratio. The two pronounced peaks between 500 and 600 nm are typical for high oxygen saturation. The absorption in the 760 nm region is characteristic for deoxy-Hb. Finally, the colorimetric *in vivo* measurement results show a more intense dark red color inside the malignant tissues (RGB data not shown but are recognizable in the VIS spectral data). The water and fat concentrations can be estimated by NIR spectral data. In tissue measurements, water is the predominant

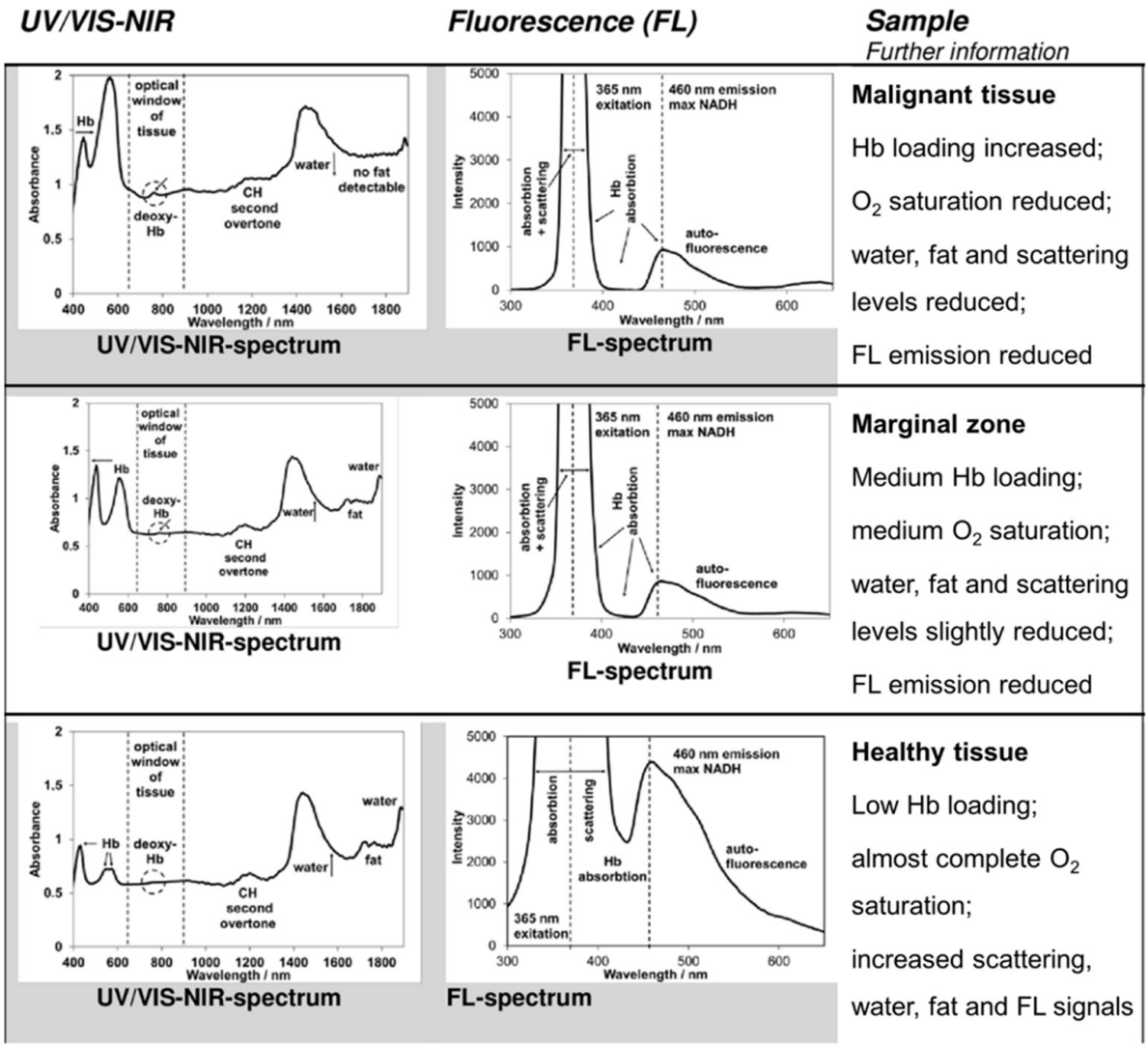

Figure 6. Exemplary *in vivo* absorbance spectra from simultaneous UV/VIS, NIR and FL spectroscopy measurements in columns 1, 2. Resulting further information added in column 3.

molecule. In our case, the O–H-stretch first overtone absorption peak at 1470 nm is too strong for quantitative analysis. The high absorption leads to very low remission signals due to artificial saturation caused by the instruments. Nevertheless, the slope at the flanks could be evaluated and demonstrated a higher water content in the healthy tissue compared with the malignant tissue. The clearly identifiable absorption in the structured region of the spectrum at approximately 1750 nm was assigned to fat (see also figure 5), which had a reduced concentration inside the tumor.

The second step in the sequence chain is the extraction of the relevant information from the whole multispectral data performed by a five-sensor photometer setup. This virtual setup is described in figure 3. This extracted data allowed the differentiation of the respective tissues using 2D PCA, shown in figure 7. Which is the third and last step in the sequence chain.

The practical applicability of the measurement system was demonstrated in an animal model ($N = 6$, female SPF NMRI mice) by penetrating the needle *in vivo* through healthy and malignant tissue (Lewis lung carcinoma cells). The recorded multispectral data are reduced by a virtual photometer setup using 10 significant channels. They result in five sensors with a total data-amount of 10 bytes per measurement point. In order to sort tissue into groups, a principal component analysis (PCA) is used. The model consists of two components, which contain 85% of the total photometric variation (PC1 = 67%/ PC2 = 18%). By comparing associated measuring changes in biochemical, physical-morphological and colorimetric values all 96 measurement points are shown. Three resulting groups—healthy, marginal and malignant tissue—are visible and highlighted in the score plot. The influence of the respective sensor is shown in the loading-plot.

The first two components explain 85% of the total photometric variation (PC1 = 67% and PC2 = 18%). The loadings represent the weighted influence of the respective virtual specialized sensors, as shown in figure 7. Exemplary for one stitch the signals of the five sensors are given in the supporting information.

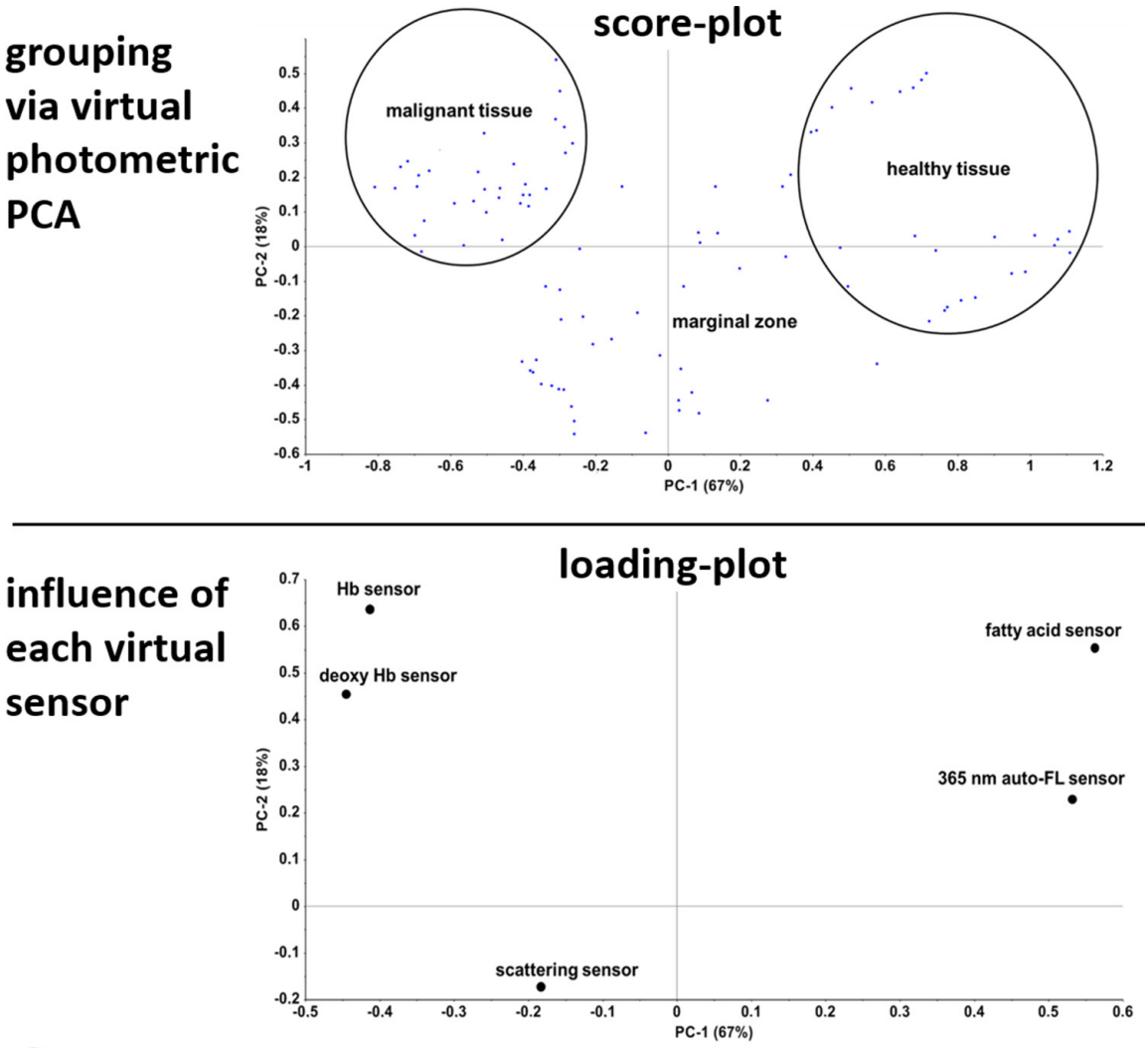

Figure 7. Principal component analysis (PCA) of the photometric data. The preprocessed and reduced information acquired from the sample points using UV/VIS, NIR and FL spectroscopy. The results are illustrated by a score- (including the highlighted classes) and a loadings-plot.

4. Discussion

Cancer is characterized by uncontrolled proliferation and therefore by excessive consumption of nutrients such as glucose, glutamine and fatty acids to support rapid growth. An overview of the fundamental pathways of nutrient acquisition and cancer metabolism has been provided by DeBerardinis and Chandel [44]. Based on these features, changes in metabolism and morphology can be diagnosed using multispectral *in vivo* spectroscopy techniques. Hb, NADH, water, fat, color, and scattering characteristics are important detectable endogenous markers. Of particular interest in blood supplied tissue of animal models is the pigment Hb. This serves as an oxygen carrier molecule (loaded and unloaded), allowing the determination of both the local oxygen saturation and the total Hb concentration. In our investigations, the oxygen concentration in tumors was reduced. Thus, the tumor was not adequately supplied with oxygen despite initiation of angiogenesis activity, which generally results in higher Hb loading in malignant tissue. Consequently, more oxygen is converted than provided from the surrounding tissue (despite better blood supply), which can result in an oxygen gradient from malignant to healthy tissue caused by diffusion, as shown in figure 6 and the supporting information. This observation supports different/increased metabolic activity inside and in the marginal zone of the evaluated tumor tissues. Fadaka *et al* [45] described a large dependence on the blood supply: 'Hypoxia and glucose shortage are rapidly generated in the inner mass of a growing tumor. In the early carcinogenesis phase, uncontrolled cell proliferation moves tumor cells away from blood vessels and, therefore, from oxygen and nutrient supply. The only way oxygen and glucose can reach the inner cells of a non-vascularized tumor is by diffusion across the basement membrane and through the peripheral tumor-cell layers.' In 1924, Warburg already proposed a hypothesis for cancer metabolism [46] in which cancer cells preferentially gain necessary energy through glycolysis upregulation, leading to the conclusion that oxygen is not inevitably necessary for cancer growth [47]. The amount of water is qualitatively higher in healthy subcutaneous tissue than in tumor tissue. The same phenomenon is valid for fat, which is reduced in tumors due to the increase in fatty acid synthesis [45]. Simultaneously,

the measured stimulated tissue autoFL in tumors with a good blood supply is more reduced in comparison to subcutaneous tissue in the immediate vicinity. However, an increase in absorption attributable to higher Hb loading in the spectral range of FL excitation and emission was measured by the introduced setup. Morphological changes were detectable by reduced backscattering in the optical window of tissue in comparison with the increase in light scattering in the surrounding healthy subcutaneous tissue. In summary, our investigations have shown that fat and water can be detected in the near NIR based on characteristic bands. Fluorophores, such as NADH, can be better observed in FL emission signals with the higher sensitivity than using absorption spectroscopy. For determining blood concentration, the characteristic bands in the visual range allow a clear interpretation. Furthermore, the scattering characteristics of the analyzed malignant tissue differ from the high scattering in the surrounding subcutaneous tissue, which can clearly be observed in the optical window of tissue.

The goal of our work was to achieve an easy to use measuring system for *in vivo* tissue analysis with high monitoring frequency. With this mind compromises in the sensor design, optical arrangement and even in the data evaluation had to be accepted. The chosen design and backscattering measurement principle allowed reduction of the clinical tool to the size of a needle. In the present study, only relative changes in concentration linked to FL emission are shown. The evaluation of absolute values for fluorophores cannot be easily conducted. However, to overcome these problems, an auto correction algorithm is required that compensates these effects. In a first step, quantitative NADH FL measurements were performed in a tissue phantom with adjustable scattering parameters [22, 36].

Diagnosis of tumorous tissue cannot be achieved solely by spectral data and an evaluation algorithm. Medically trained personnel must provide input as to whether (and to what extent) changes in a tissue deviate from normal values, regardless of whether the values are for fat, blood concentration, color, scattering characteristics, water content, oxygen saturation, metabolic intermediates (such as NADH) or other values and symptoms that provide clinical evidence. More correlations with histological changes are needed in the future.

5. Summary and conclusion

The basic idea of the presented work was to develop a setup that can simultaneously detect various spectroscopic techniques (UV/VIS, NIR, FL) for the detection and evaluation of malignant tissue in real-time. The setup was composed of a customized multispectral needle probe and an integrated set of different light sources as well as spectrometers all of which are described in detail. The head of the multispectral needle has an optimized shape especially for *in vivo* measurements. The measured data were processed by a virtual photometric setup and combined and clustered into groups. To handle the recorded spectral data, a virtual photometer converts spectral data into channels and in a next step into sensors. These specific sensors explain change-related tissue alterations by monitoring morphological properties and metabolic parameters: Hb, deoxy Hb, scattering, fat and auto FL. In a next sequence the information of each channel are the variables of a 2D PCA. This analysis allows a grouping of 96 label-free measurement points generated *in vivo*. The first two components of the PCA explain 85% of the total photometric variation. All samples can be clearly attributed to three groups (malignant, marginal and healthy tissue) visible in the PCA score-plot. This goal was successfully accomplished in a mouse tumor model (Lewis lung carcinoma) and verified by classical histology.

5.1. Scope and potential future application

The applied methods and the reported results are highly promising and will serve as an entry point for potential future directions. Our goals for the development of the probe setup and evaluation system are multiple use, easy cleaning, sterilization capability, and professional (i.e. commercial) applicability. The typical conventional biopsy procedure requires up to 24 core saturation tissue fragments (biopsy to obtain tissue samples in a systematic manner). This process supported by the optical needle could reduce the number of samples collected. As a result, histology costs could be lowered together with the benefit of a real-time preselection during the procedure guided by ultrasound or MRI. Currently, a cancer is diagnosed by a combination of results from different techniques and disciplines: detection of cancerous tissue, localization, tissue sampling, biopsy and verification by a specialist/pathologist. In general, this sequence is time consuming. Our goal is to allow smart real-time *in vivo* detection and to facilitate the work of medical personnel by providing them with multispectral pre-information during the procedure. By using our setup, morphological, metabolic and other PCA parameters are immediately available *in vivo*, allowing a secure diagnosis in combination with of medical knowledge. In future work, the presented setup will be tested for the investigation of other cancer types or other medically relevant tissue changes such as inflammation. The optical measurement head is applicable for analysis *in vivo*. Various steps for optimization and application of the fiber optic needle are planned: advanced materials will be used for the probe head (e.g. hardened or hard metal or ceramic) with the benefit of multiple needle uses without grinding, development of a disposable probe based on plastic and polymer optical fibers to avoid cleaning and sterilization procedures. The use of further fibers as backup channels are planned. Those lead to higher safety integrity and an increased availability by hot-spare redundancy. Finally, an aim in the future is the implementation of Raman measurements using a sensitive spectrometer with adjustable resolution and implemented filter units for high photon flux [48]. This technique will increase the multispectral information. This approach may provide access to assessment of other key molecules: ATP, glutamine, glucose, and lactic acid (lower glucose and higher lactic acid concentrations are observed in the tumor microenvironment [49]). Exogenous fluorophores are also

detectable using a suitable excitation light-source, regardless of whether it is static or tunable. The fields of application will be expanded through the use of endogenous or exogenous labeling with FL marker molecules, such as indocyanine green (ICG), PpIX, and sinistrin, which has a demonstrated potential for determination of glomerular filtration rate (GFR) [50, 51]).

Furthermore, reduction of the necessary instrumentation effort by lowering the recorded number of wavelengths is possible. The elaborated method can be integrated into robust, compact and low-cost embedded computing systems, photometric setups with appropriate bandpass filters, light sources and sensitive detectors. Egly *et al* [52] presented a compact multichannel FL sensor equipped with ambient light suppression through a lock-in procedure that resulted in detection limits of 4×10^{-11} mol l^{-1} and 4×10^{-9} mol l^{-1} for the fluorophores PpIX and NADH, respectively [51]. Our goal is to develop a self-learning instrument including an adapted algorithm introduced by Garcia *et al* [53] that combines diagnostics and therapy to assist medical doctors and pathologists. Their experience, interpretation and knowledge of a patient's clinical status, combined with the aforementioned fiber optic setup, will result in a smart *in vivo* human-sensor expert system for rapid grouping and characterization of tissue, followed by potential curative treatment and therapy.

Acknowledgment

This work was funded by the German Federation of Industrial Research Associations (AiF Project GmbH). The authors would especially like to express their thanks to Julia Seltenreich (University of Applied Sciences, Mannheim, Germany) and Viktoria Skude (Medical Research Center, University of Heidelberg, Mannheim, Germany) for support during the multispectral *in vivo* measurements.

Notes

Frank Braun, Norbert Gretz and Matthias Rädle are the inventors and have submitted a patent application regarding the described needle probe (DE102014107342A1).

ORCID iDs

Frank Braun https://orcid.org/0000-0002-2906-8493

References

[1] Ferlay J *et al* 2012 Cancer incidence and mortality worldwide *GLOBOCAN 2012 v1.0 IARC Cancer Base* No. 11 (International Agency for Research on Cancer, Lyon)

[2] Bray F, Jemal A, Grey N, Ferlay J and Forman D 2012 Global cancer transitions according to the human development index (2008–2030): a population-based study *Lancet Oncol.* **13** 790–801

[3] Galanski M and Lackner K 2006 Prinzipien der bildgebenden Diagnostik in der Onkologie *Kompendium internistische Onkologie: Standards in Diagnostik und Therapie* ed H J Schmoll, K Höffken, K Possinger (Heidelberg: Springer) pp 429–48

[4] Hefti F and Jundt G 2006 Grundsätzliches zur Tumordiagnostik *Kinderorthopädie in der Praxis* (Heidelberg: Springer) pp 583–93

[5] Hesse S, Leve J, Goerdeler P and Zapp W 2013 Benchmarking im Krankenhaus (Wiesbaden: Springer Gabler) (https://doi.org/10.1007/978-3-658-04134-2)

[6] Synytsya A *et al* 2004 Raman spectroscopy of tissue samples irradiated by protons *Int. J. Radiat. Biol.* **80** 581–91

[7] Krishna C M *et al* 2007 FTIR and Raman microspectroscopy of normal, benign, and malignant formalin-fixed ovarian tissues *Anal. Bioanal. Chem.* **387** 1649–56

[8] Lyng F, Gazi E and Gardner P 2011 Preparation of tissues and cells for infrared and Raman spectroscopy and imaging *Biomedical Applications of Synchrotron Infrared Microspectroscopy* ed D Moss (London: Royal Society of Chemistry) pp 147–91

[9] Kondepati V R, Heise H M and Backhaus J 2008 Recent applications of near-infrared spectroscopy in cancer diagnosis and therapy *Anal. Bioanal. Chem.* **390** 125–39

[10] Kondepati V R *et al* 2007 CH-overtone regions as diagnostic markers for near-infrared spectroscopic diagnosis of primary cancers in human pancreas and colorectal tissue *Anal. Bioanal. Chem.* **387** 1633–41

[11] Ali J H, Wang W B, Zevallos M and Alfano R R 2004 Near infrared spectroscopy and imaging to probe differences in water content in normal and cancer human prostate tissues *Technol. Cancer Res. Treat.* **3** 491–7

[12] Cerussi A, Shah N, Hsiang D, Durkin A, Butler J and Tromberg B J 2006 *In vivo* absorption, scattering, and physiologic properties of 58 malignant breast tumors determined by broadband diffuse optical spectroscopy *J. Biomed. Opt.* **11** 044005

[13] Kukreti S, Cerussi A, Tromberg B and Gratton E 2008 Intrinsic near-infrared spectroscopic markers of breast tumors *Dis. Markers* **25** 281–90

[14] Brancaleon L, Durkin A J, Tu J H, Menaker G, Fallon J D and Kollias N 2001 *In vivo* fluorescence spectroscopy of nonmelanoma skin cancer *Photochem. Photobiol.* **73** 178–83

[15] Butte P V, Mamelak A N, Nuno M, Bannykh S I, Black K L and Marcu L 2011 Fluorescence lifetime spectroscopy for guided therapy of brain tumors *NeuroImage* **54** 125–35

[16] Cheng X, Mao J M, Bush R, Kopans D B, Moore R H and Chorlton M 2003 Breast cancer detection by mapping hemoglobin concentration and oxygen saturation *Appl. Opt.* **42** 6412–21

[17] Vaupel P, Mayer A and Höckel M 2008 Relationship between hemoglobin levels and tumor oxygenation *Recombinant Human Erythropoietin (rhEPO) in Clinical Oncology: Scientific and Clinical Aspects of Anemia in Cancer* (Vienna: Springer) pp 265–82

[18] Almog N 2010 Molecular mechanisms underlying tumor dormancy *Cancer Lett.* **294** 139–46

[19] Chen P, Fernald B and Lin W 2011 Estimation of regional hemoglobin concentration in biological tissues using diffuse reflectance spectroscopy with a novel spectral interpretation algorithm *Phys. Med. Biol.* **56** 3985–4000

[20] Kragh M, Quistorff B, Lund E L and Kristjansen P E 2001 Quantitative estimates of vascularity in solid tumors by non-invasive near-infrared spectroscopy *Neoplasia* **3** 324–30

[21] Pu Y, Shi L, Pratavieira S and Alfano R 2013 Two-photon excitation microscopy using the second singlet state of fluorescent agents within the 'tissue optical window' *J. Appl. Phys.* **114** 153102
[22] Braun F *et al* 2017 NADH-fluorescence scattering correction for absolute concentration determination in a liquid tissue phantom using a novel multispectral magnetic-resonance-imaging-compatible needle probe *Meas. Sci. Technol.* **28** 075903
[23] Fritsch C, Becker-Wegerich P M, Menke H, Ruzicka T, Goerz G and Olbrisch R R 1997 Successful surgery of multiple recurrent basal cell carcinomas guided by photodynamic diagnosis *Aesthetic Plast. Surg.* **21** 437–9
[24] Kriegmair M, Baumgartner R, Knuchel R, Stepp H, Hofstadter F and Hofstetter A 1996 Detection of early bladder cancer by 5-aminolevulinic acid induced porphyrin fluorescence *J. Urol.* **155** 105–9 (discussion 109–10)
[25] Baumgartner R *et al* 1996 Inhalation of 5-aminolevulinic acid: a new technique for fluorescence detection of early stage lung cancer *J. Photochem. Photobiol.* B **36** 169–74
[26] Lohmann W, Mussmann J, Lohmann C and Kunzel W 1989 Native fluorescence of the cervix uteri as a marker for dysplasia and invasive carcinoma *Eur. J. Obstet. Gynecol. Reprod. Biol.* **31** 249–53
[27] Eng J, Lynch R M and Balaban R S 1989 Nicotinamide adenine dinucleotide fluorescence spectroscopy and imaging of isolated cardiac myocytes *Biophys. J.* **55** 621–30
[28] Pradhan A *et al* 1995 Steady state and time-resolved fluorescence properties of metastatic and non-metastatic malignant cells from different species *J. Photochem. Photobiol.* B **31** 101–12
[29] Ramanujam N 2000 Fluorescence spectroscopy of neoplastic and non-neoplastic tissues *Neoplasia* **2** 89–117
[30] Kollias N, Zonios G and Stamatas G N 2002 Fluorescence spectroscopy of skin *Vib. Spectrosc.* **28** 17–23
[31] Heikal A A 2010 Intracellular coenzymes as natural biomarkers for metabolic activities and mitochondrial anomalies *Biomark Med.* **4** 241–63
[32] Piston D W, Masters B R and Webb W W 1995 Three-dimensionally resolved NAD(P)H cellular metabolic redox imaging of the *in situ* cornea with two-photon excitation laser scanning microscopy *J. Microsc.* **1** 20–7
[33] Dora E, Gyulai L and Kovach A G 1984 Determinants of brain activation-induced cortical NAD/NADH responses *in vivo* *Brain Res.* **299** 61–72
[34] Mayevsky A, Doron A, Manor T, Meilin S, Zarchin N and Ouaknine G E 1996 Cortical spreading depression recorded from the human brain using a multiparametric monitoring system *Brain Res.* **740** 268–74
[35] Georgakoudi I *et al* 2002 NAD(P)H and collagen as *in vivo* quantitative fluorescent biomarkers of epithelial precancerous changes *Cancer Res.* **62** 682–7
[36] Braun F, Heintz A, Schalk R, Beuermann T, Gretz N and Rädle M 2018 NADH-fluorescence absorption correction to determine absolute fluorophore concentrations of a liquid tissue model *Meas. Sci. Technol.* **29** 107001
[37] Pelton A, Stöckel D and Duerig T 2000 Medical uses of nitinol *Mater. Sci. Forum* **327–8** 63–70
[38] Duerig T, Pelton A and Stöckel D 1999 An overview of nitinol medical applications *Mater. Sci. Eng.* A **273–5** 149–60
[39] Morgan N B 2004 Medical shape memory alloy applications—the market and its products *Mater. Sci. Eng.* A **378** 16–23
[40] Braun F, Gretz N and Rädle M 2015 Vorrichtung und Verfahren zur Erkennung von Krebstumoren und anderen Gewebeveränderungen *German Patent* DE 10 2014 107 342 A1
[41] Kessler W 2007 *Multivariate Datenanalyse* (Weinheim: Wiley-VCH) (https://www.wiley-vch.de/de/fachgebiete/naturwissenschaften/multivariate-datenanalyse-978-3-527-31262-7)
[42] Büning-Pfaue H 2003 Analysis of water in food by near infrared spectroscopy *Food Chem.* **82** 107–15
[43] Wilson R H, Nadeau K P, Jaworski F B, Tromberg B J and Durkin A J 2015 Review of short-wave infrared spectroscopy and imaging methods for biological tissue characterization *J. Biomed. Opt.* **20** 030901
[44] DeBerardinis R J and Chandel N S 2016 Fundamentals of cancer metabolism *Sci. Adv.* **2** e1600200
[45] Fadaka A, Ajiboye B, Ojo O, Adewale O, Olayide I and Emuowhochere R 2017 Biology of glucose metabolization in cancer cells *J. Oncol. Sci.* **3** 45–51
[46] Warburg O, Wind F and Negelein E 1927 The metabolism of tumors in the body *J. Gen. Physiol.* **8** 519–30
[47] Gatenby R A and Gillies R J 2004 Why do cancers have high aerobic glycolysis? *Nat. Rev. Cancer* **4** 891–9
[48] Braun F *et al* 2016 Highly sensitive raman spectroscopy with low laser power for fast in-line reaction and multiphase flow monitoring *Anal. Chem.* **88** 9368–74
[49] Jiang B 2017 Aerobic glycolysis and high level of lactate in cancer metabolism and microenvironment *Genes Dis.* **4** 25–7
[50] Steinbach S *et al* 2014 A pilot study to assess the feasibility of transcutaneous glomerular filtration rate measurement using fluorescence-labelled sinistrin in dogs and cats *PLoS One* **9** e111734
[51] Moggio A, Geraci S, Boido A, Sticht C, Gretz N and Bussolati B 2017 Assessment of acute kidney injury in rhabdomyolytic mice by transcutaneous measurement of sinistrin excretion *Nephrol. Dial. Transplant.* **32** 1167–75
[52] Egly D, Geörg D, Rädle M and Beuermann T 2012 A compact multi-channel fluorescence sensor with ambient light suppression *Meas. Sci. Technol.* **23** 035702
[53] Molina J F G, Zheng L, Sertdemir M, Dinter D J, Schonberg S and Radle M 2014 Incremental learning with SVM for multimodal classification of prostatic adenocarcinoma *PLoS One* **9** e93600